31st Congress of the International Council of the Aeronautical Sciences

Belo Horizonte, Brazil; September 09-14, 2018

THE INFLUENCE OF HIGH-SPEED SPIV DATA PROCESSING PARAMETERS ON AIRCRAFT WING VORTEX WAKE ASSESSMENT

Kevin Garry*, Davide Di Pasquale*, Simon Prince* & Nicholas J. Lawson*
***Cranfield University, UK**

Keywords: *High-Lift, Wake vortex, SPIV*

Abstract

This paper uses Stereoscopic Particle Image Velocimetry (SPIV) data from the near wake of a detailed sub-scale ½ model of a representative transport aircraft wing with leading and trailing edge high lift systems and outboard aileron representation, to analyse the influence of data-sampling period and frequency on the magnitude and position of the vortices resolved within the wake. The paper also evaluates the extent of vortex 'wander' at various stages of development within the near wake and offers guidance for optimum time-averaging strategy when investigating complex longitudinal vortex interaction studies in similar flow fields.

1 Introduction

A counter-rotating vortex system forms behind any aircraft fixed wing. Wingtip vortices are extremely important phenomena in fluid dynamics for their negative effects in many applications. This vortex system persists for a long distance downstream, which represents a considerable hazard for any following aircraft. The consequence is that the schedule of take-offs and landings at airports must be managed to give time for these vortices to dissipate. There are two approaches to produce less harmful wake vortices. The first one is to generate vortices with lower maximum vorticity and the largest vortex radius that is possible. The other is to generate vortices with as high a decay rate of circulation as possible at a given wake age. Both these approaches need a better understanding of the physics of the wake vortex system, which is now still insufficient. The development of the wake structure downstream of a transport aircraft wing is, therefore, of significant interest to those concerned, for example, with the aerodynamic load development on the wing or the aeroacoustics characteristics of the wing high lift systems and control surfaces. Wind tunnel simulations with sub-scale models using Stereoscopic Particle Image Velocimetry (SPIV) has proved to be a powerful tool in the measurement of the detailed flow structure within such flow fields, allowing decomposition of local flow velocity vectors at high sampling rates. The development of the trailing vortex system along such wings have revealed the formation of several secondary vortices which interact with the primary tip vortex, generating low frequency fluctuations [1]. The high spatial resolution achieved by the SPIV technique has allowed a deeper understanding of the vortex structure in the early wake and the turbulence production and dissipation within the vortex core. The majority of SPIV studies of this type have presented time-averaged flow velocity data which is the result of ensemble averaging of a number of consecutive images at an appropriate flow seeding density and level of optical illumination. The resulting data reveal the time-averaged strength and location of longitudinal vortices embedded within the wake, but current high-speed SPIV systems allow instantaneous characteristics to be analysed. In this paper SPIV experiments were carried out to study wing tip vortex and aileron vortex interaction of a representative transport aircraft wing. Different methods of vortex identification based on SPIV results were compared to identify the vortex core, and its motion, more effectively.

1.1 Vortex Flows

A Vortex is a significant phenomenon in fluid mechanics. The conceptual notion of a vortex usually refers to a tube-like structure with persistent and coherent rotation about its core. However, a clear definition of a vortex is still lacking. Several authors proposed different descriptions [2, 3, 4, 5, 6]. The distribution of velocity, vorticity and circulation are three main factors to characterize the vortex.

Vorticity (ω) is defined as twice the angular velocity and can also be expressed as the curl of the velocity in a velocity field. Consider a velocity field in Cartesian coordinate:

$$V = V(x, y, x) \qquad (1)$$

The vorticity is:

$$\omega = \nabla \times V = \\ = \left(\frac{\partial V_z}{\partial y} - \frac{\partial V_y}{\partial z}\right) i + \left(\frac{\partial V_x}{\partial z} - \frac{\partial V_z}{\partial x}\right) j + \left(\frac{\partial V_y}{\partial x} - \frac{\partial V_x}{\partial y}\right) k \qquad (2)$$

If $\nabla \times V = 0$ at every point in a flow, the flow is called irrotational, which implies that there is no angular velocity. If $\nabla \times V \neq 0$ at every point in a flow, the flow is called rotational, which implies that the flow elements have a finite angular velocity. Circulation, Γ, is defined as the negative of the line integral around a closed curve, *C*, of incremental length *ds*, of velocity, *V*. It is a kinematic property and only depends on the velocity field and choice of the curve, and is given by:

$$\Gamma = -\oint_C V ds \qquad (3)$$

Circulation is also related to vorticity from Stokes' theorem as follows:

$$\Gamma = -\oint_C V ds = \iint_S (\nabla \times V) dS \qquad (4)$$

where *dS* is the incremental area of the surface segment. Hence, the circulation about a curve *C* is equal to the vorticity integrated over any open surface bounded by curve *C*.

Vorticity contours are used to obtain the vortex centre. Circulation decreases with increasing radius. Vortex cores are regions of intense low pressure. The radius with respect to the maximum velocity is defined as the vortex core radius. Within the vortex core, tangential velocity increases with increasing radius and vice versa. Vortex cores, according to [7], have the following properties:

- A vortex core must have a net vorticity (hence, net circulation). Thus, potential regions are excluded from vortex core regions, and a potential vortex is a vortex with zero cross section.
- The geometry of the identified vortex core should satisfy Galilean invariance, which means the vortex core must be the same in all inertial frames.

2 Vortex Identification

Particle image velocimetry (PIV) is a key measurement technique to study turbulent flow in a research laboratory [8]. Using this method, the velocity field can be obtained, from which vorticity distribution can be calculated. However, vorticity cannot be used to identify and track vortical structures in all circumstances. Other vortex identification methods need to be introduced. This study relates to the use of particle image velocimetry to analyse the wake structure from a wing tip and aileron. As a consequence only vortex identification methods directly related to velocity field information will be discussed in this paper.

2.1 Vorticity method

As mentioned above, Vorticity, ω, is defined as twice the angular velocity and can also be expressed as the curl of the velocity in a velocity field. Because of this, vorticity can be used to identify vortices directly. Kim et al. (1987) proposed the isosurface of vorticity magnitude method and the local clustering of vortex lines method to track vortices [9]. These are detailed in the following sections. By plotting isosurfaces of vorticity magnitude, vortices can be identified. Different vorticity thresholds result in different geometric vortex structures. A vortex is stretched

along a velocity gradient, and the vorticity magnitude will increase, which is known as vortex stretching.

2.2 Vortex Interaction

In the near wake of a lifting transport aircraft wing, a series of co-rotating wing vortices interact and may merge into the wing tip vortex. As a result of these merging processes each wing of the aircraft generate one predominant tip vortex. These two, conter-rotating, equal-strength vortices remain stable in the wake far field for a prolonged period before developing medium- and long-wavelength instabilities, e.g., of 'Crow' mode [10]. An early disintegration of this vortex pair can be caused by an asymmetry in vortex strength introduced, for example, by control surface deployments which generate their own vortices. A better understanding of the interaction of main tip and secondary control surface vortices in the wake is, therefore, needed.

3 Experiment Details

The SPIV measurements were made in the Cranfield University, 2.4m x 1.8m closed working section, low speed, wind tunnel in the Reynolds number range $1.41 \times 10^6 < Re/m < 3.18 \times 10^6$. The wind tunnel model, shown in Fig 1, was a $1/17^{th}$ scale wing on a half body (semi-span, b = 1.312m) based on the Airbus NEXUS 46 wing design with a Kuchemann tip and a 1-g flight shape.

The wing could be configured in a high lift configuration with high-lift devices deployed (leading edge slat 22deg, trailing edge flap 16deg). This high lift configuration was used throughout the tests reported in this paper. The wing was fitted with an interchangeable solid outboard aileron, which could be set at 0 or 10 degrees deflection to assess aileron edge vortices, as shown in Fig 2.

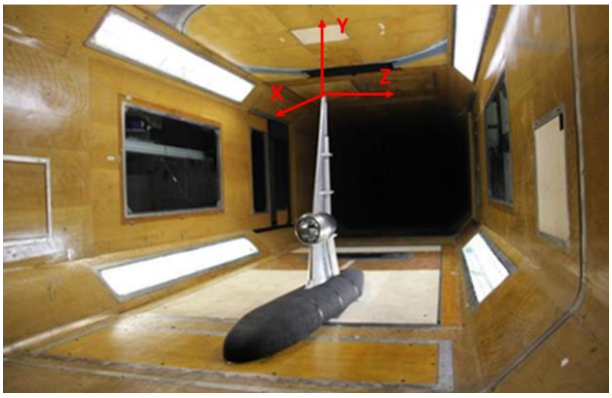

Fig 1: Wind tunnel model viewed from upstream

Fig 2: Photo of the aileron and trailing edge flap

A through-flow nacelle and pylon is used together with a simple half body representation (with nominal dimensions corresponding to that of the A321 fuselage) that can be set at a range of angles, α, relative to the free stream. All the measurements reported here were undertaken at α = 6.4deg. SPIV data was recorded in planes orthogonal to the free stream in the range $0.303b < z < 1.163b$ downstream of the wing tip. Fig 3 presents the laser light sheet downstream of the model in the wind tunnel.

The two SPIV 16 bit cameras (LAVision Imager sCMOS) were mounted externally viewing the image plane at an angle of 45 degrees through the test section side windows. Laser light sheet illumination was provided by a Litron TRL425-10 laser system mounted beneath the wind tunnel working section, and the model axial position adjusted to vary the downstream distance of the measurement plane from the model.

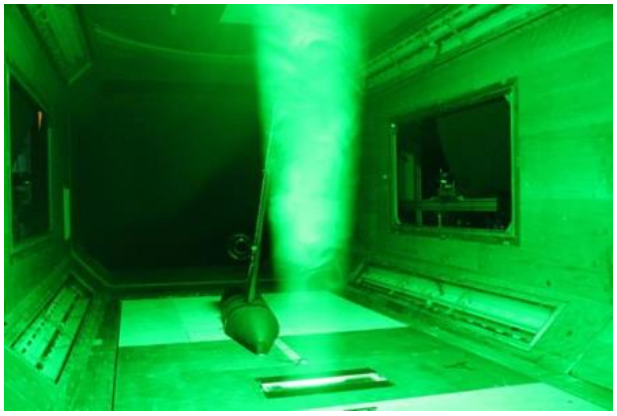

Fig 3 : SPIV laser illumination sheet depicted, from downstream

At each test condition, the sampling frequency was 10Hz and 100 seconds of data was acquired. Each data set therefore contained 1000 sequential frames of 3-component velocity data. Only the first 800 frames were used for the analysis because of a lack of confidence in the temporal scheduling of the data during the last 20 seconds as a result of data-transfer limitations within the DAQ system. The axis reference point was the wing tip trailing edge, and Table 1 presents the location of the key wing features.

Table 1: The relative positions of wing geometry (relative to wing tip)

	Wingtip	Aileron (outboard tip)	Aileron (inboard tip)	Flap (outboard tip)	Crank
x(mm)	0	-5	-28	-29	-68
y(mm)	0	-53.5	-287	-293.3	-810.2

The free-stream velocity for the cases investigated was constant at V_∞ = 45m/s. Sequences of the vortex core size, vortex centre position and circulation downstream were investigated for different configurations. The parameters of each configuration are presented in Table 2. The *z* distance refers to the axial location of the laser light sheet downstream of the wing tip trailing edge.

Table 2: Experimental parameters setting

Aileron deflection	0°	10°	-	-
z Distance (mm)	398	718	1122	1520
Velocity (m/s)	20	32	45	-

4 Post-Process Methodology

Preliminary post processing of the SPIV data was previously undertaken using DaVIS vr8.2 proprietary software package. The resulting raw velocity data files were imported into MATLAB and the functions 'Meshgrid' and 'Griddata' used to generate suitable data grids. 'Meshgrid' creates a two-dimensional grid with uniformly spaced *x*-coordinates and *y*-coordinates, and 'Griddata' interpolates scattered data [11]. In this case, the 'nearest' interpolation method has been used, because of the missing data at some points in the raw data.

4.1 Replacing missing Data and smoothing data

Stereoscopic particle image velocimetry in it's simplest form obtains non-intrusive, planar three-component instantaneous velocity data, from a pulsed laser light sheet, placed in the fluid area of interest which is seeded with solid or liquid particles. The main source of PIV errors includes Gaussian noise from the images and correlation noise from the data processing which leads to outliers and missing data in the plane of interest. These errors affect velocity distribution and flow quantities based on velocity distribution such as vorticity and circulation. Therefore, before analysing PIV data, post-processing algorithms need to be used. For this case two post-processing algorithms have been tested, the DCT–PLS method, proposed by Garcia [12, 13] and the POD method. The DCT-PLS method which is based on a Penalized Least Squares (PLS) approach, the Discrete Cosine Transform (DCT) and the generalized cross-validation, and thus allows fast removal of noise, replacing of missing data and outliers of PIV data automatically. Both methods can be used to detect the outliers, replace the incorrect and missing values and smooth data. But comparing the results between the two methods, the DCT-PLS method fills the gap more effectively than the POD method, as shown in Fig 4 and Fig 5. The DCT-PLS approach is time independent. It can deal with this problem relative easily and is significantly quicker than the POD method to implement.

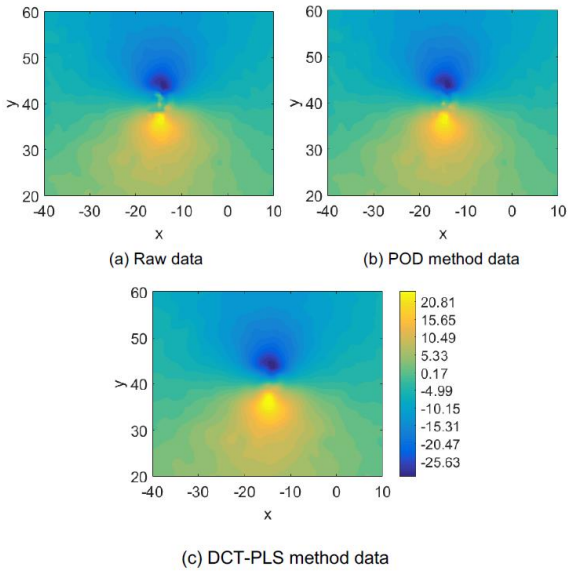

Fig 4 : Comparison of u velocity contour via the different methods [14]

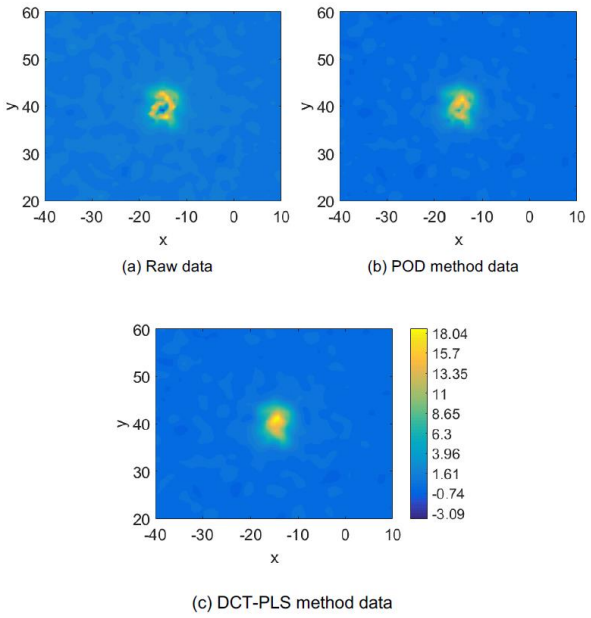

Fig 5 : Comparison of vorticity contour via the different methods [14]

4.3 Vortex identification method

Various vortex identification methods are carried out using Matlab. Specifically, the vorticity contour method, the Q-criterion method, which represents the local balance shear strain rate and vorticity magnitude and the Δ-criterion method, including the λ_{ci} and λ_2 [15]. As velocity is no more than 45m/s, the freestream Mach number is nominally 0.13, it can be regarded as an incompressible flow. An idealised Lamb-Oseen vortex [16] was created to investigate the accuracy of these vortex identification methods. The circulation contained in the sample vortex is $15m^2/s$ and the vortex core diameter is 5m. In order to have a clear vortex core region, eight contour levels were used in all plots. It can be seen from Fig 6 that the vorticity method provides a larger vortex core region compared to the other methods. This is because in the vorticity method a threshold value for the vortex core region needs to be identified.

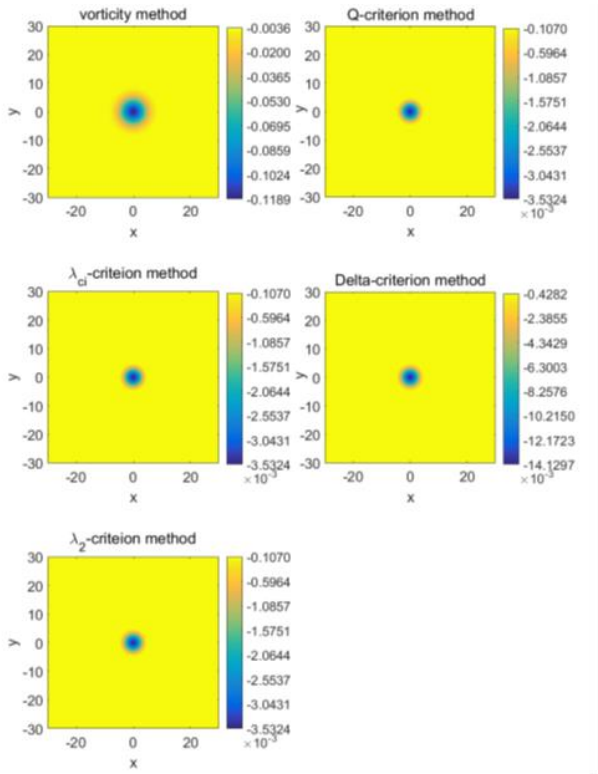

Fig 6: Comparison of different vortex identification methods [14]

4.4 Vortex centre identification

The velocity sign method, vorticity method and Q method have been applied in the study. Maximum vorticity is another method that can be used to identify the vortex centre. However, although missing data in the vortex core can be addressed as outlined in the previous section, this process may cause some uncertainty when identifying the position of maximum vorticity value. The velocity sign method detects the

inversion point for *u* and *v* velocities. Holmen (2012) introduced this method, which is explained in [17]. After applying all three methods, it was concluded that all three result in some errors. However, the maximum error is no more than the width of the grid. The Q method is better when compared with the vorticity method. The velocity sign method is suitable when the mesh width is smaller. The Q method is suitable for the case when mesh width is larger.

5 Results and Analysis

The vortex centre movement along the longitudinal axis for both aileron deflected (10 degree) on and aileron zero deflection cases has been analysed and the vortex identification methods have been used to analyse the change in the size of these vortices along the longitudinal axis. The influence of the aileron vortex and the merging process of the aileron vortex and the wing tip vortex has also been investigated and the corresponding vortex circulations are computed and compared. The complexity of the near wake structure downstream of the aileron and trailing edge flap is depicted by the composite time-averaged SPIV axial velocity data, as shown in Figure 7.

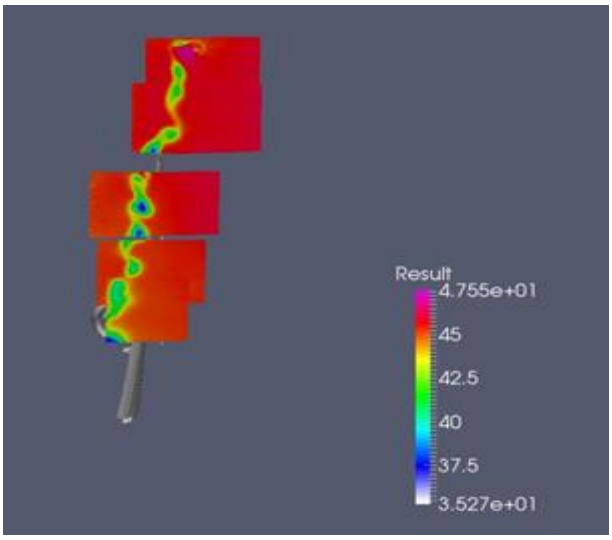

Figure 7: composite time-averaged SPIV axial velocity data

5.1 Vortex centre movement

An averaging operation for the 800 time frames for each configuration was carried out before doing the analysis. Although results for the different methods showed only small differences, (no more than 3mm at model scale), they show the same trend for the movement of the centre of the wing tip vortex. For the first case, i.e. 0^o aileron deflection, the tip vortex moves downwards and inwards at the same time as it convects downstream. For the 10^o aileron deflection case, the tip vortex moves in the same direction. However, the tip vortex moves further outboard (+ve y direction) and closer (upwards) in the *x* direction. This is assumed to be because the interaction process makes the tip vortex and the aileron vortex converge and suppresses the sinking of the tip vortex.

Tables 3 and 4 present the measured tip vortex centre locations obtained using the different identification methods for the zero and ten degree aileron configurations respectively.

Table 3: Trajectory of centre of tip vortex downstream using different vortex centre identification methods for 0^o aileron deflection

Method		Q		Vorticity		Velocity Sign	
V_∞	z(mm)	y(mm)	x(mm)	y(mm)	x(mm)	y(mm)	x(mm)
45 m/s	398	-23.10	-49.85	-23.16	-49.806	-24.30	-50.02
	718	-33.74	-75.46	-33.78	-75.45	-34.66	-75.37
	1122	-58.45	-107.79	-58.65	-107.71	-58.58	-107.78
	1520	-76.16	-146.53	-76.46	-146.49	-77.35	-146.29

Table 4: Trajectory of centre of tip vortex downstream using different vortex centre identification methods for 10^o aileron deflection

Method		Q		Vorticity		Velocity Sign	
V_∞	z(mm)	y(mm)	x(mm)	y(mm)	x(mm)	y(mm)	x(mm)
45 m/s	398	-30.84	-50.47	-30.69	-50.55	-32.87	-50.02
	718	-42.34	-69.41	-42.44	-69.36	-43.23	-70.37
	1122	-71.76	-97.13	-71.71	-97.10	-73.34	-98.23
	1520	-85.8	-128.62	-85.64	-128.73	-87.31	-128.82

5.2 Vortex visualisation

Fig 8 presents the computed vorticity contours at four *x-y* planes downstream of the wing tip trailing edge, for the zero deflection aileron case. The tip vortex is seen to move inboard, in the minus *y* direction as well as downwards, in minus *x* direction, as it proceeds downstream.

The maximum vorticity value can be considered as the strength of the swirling motion. The maximum vorticity value along the *z* (stream-wise) direction becomes progressively smaller, which means that the swirling strength decreases as the vortex travels downstream.

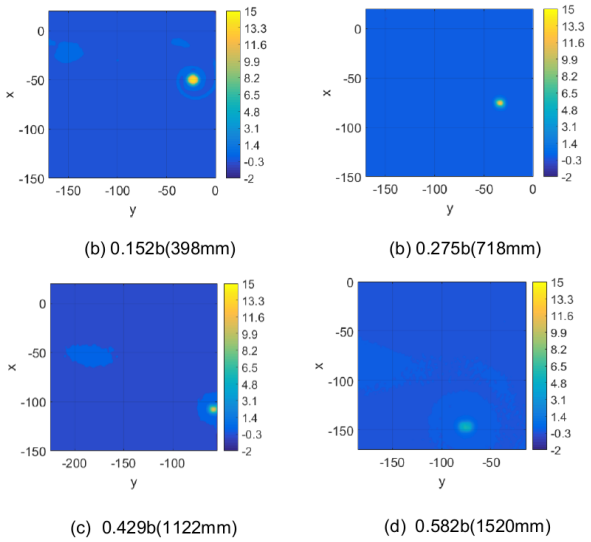

Fig 8: Vorticity contour downstream at four z-planes downstream, for 0^o aileron deflection

Fig 10 presents the corresponding vorticity contours downstream for the 10 degree aileron deflection case. The vortex motion is seen to be similar, ie: the tip vortex moves inboard, in the minus *y* direction, and in the downwards, minus *x*, direction at the same time as it convects downstream.

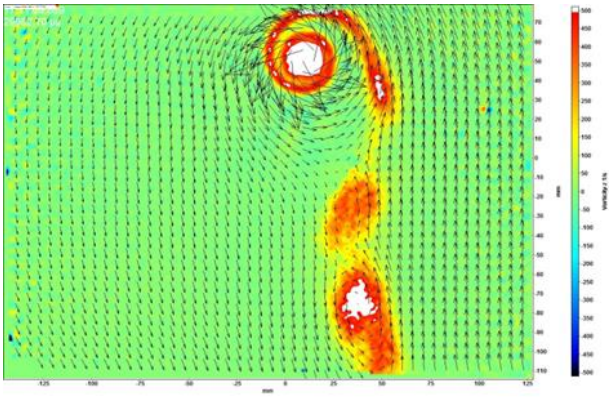

Fig 9: Time-averaged vorticity (ζ, /s) distribution in a plane orthogonal to the free stream 0.303b downstream of the wing tip, zero outboard aileron deflection.

The main difference is that in the longitudinal position in the range *z* = 0.125 to 0.275*b* (0.398m-0.718m) behind the wing, the aileron vortex can be identified at each measurement plane. The aileron vortex rotates around the tip vortex anti-clockwise. The aileron vortex disappears within the range from *z* = 0.429 to 0.582 span (1.122 m-1.52m).

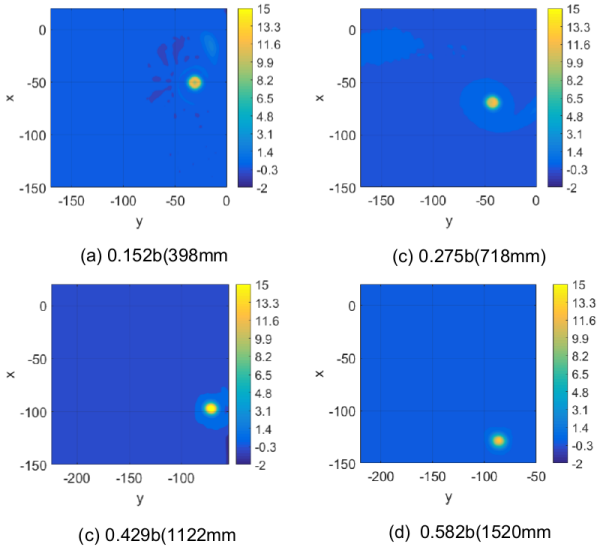

Fig 10: Vorticity contour downstream for 10^o aileron deflection

This phenomenon could be due to two possible causes. First, looking at Figure 10c, it is possible to see that the tip vortex is located at the edge within the frame captured by the camera thus the aileron vortex which rotates around the tip vortex may not have been captured. The second reason is that the merging process might have been completed before *z* = 0.429*b*, therefore only the tip vortex exists in the plane. The maximum vorticity value which represents the swirling strength becomes smaller in the range 0.125 to 0.275*b* (0.398m-0.718m) and then increases to the maximum value in the range 0.275 to 0.429*b* (0.718m-1.122m), after which it decreases again (1.122m-1.52m). This means that the vortex merging process has probably been completed before z = 0.429*b*. To be specific, the newly merged vortex contains higher energy, which could come from the combination of both the tip vortex and the aileron vortex so that the maximum vorticity value in Figure 10c is the largest of the four figures. To investigate how the

vortices propagate in the longitudinal direction, several vortex identification methods were employed. However, only one vortex could be identified from the contour data - the other possible vortices could not be identified. This is assumed to be because the intensity of these vortices was too small to be resolved in the contour plots. Therefore, all the criterion for all the methods need to be adjusted to detect those missing vortices that have lower intensity in the contour plots.

5.3 Circulation

It was found that the circulation within the tip vortex of the 10° aileron deflection case was higher than that for the corresponding 0° aileron deflection case. For 0° aileron deflection, the circulation at 0.152*b* (398mm) was the highest, and this then decreases dramatically by 0.275*b*, after which the circulation increases slowly as the vortex progresses downstream. The minimum circulation appears at $z = 0.275b$ because the size of the tip vortex here is the smallest, as shown in Fig 11. As for the other case, circulation fluctuates, reaching a maximum at $z = 0.429$b (1122mm). It can be found that the existence of the aileron vortex increases the circulation of the tip vortex. As mentioned above, the tip vortex and aileron vortex appear to have merged by the time they reach $z = 0.429b$, and because of this the circulation reaches its maximum around this station.

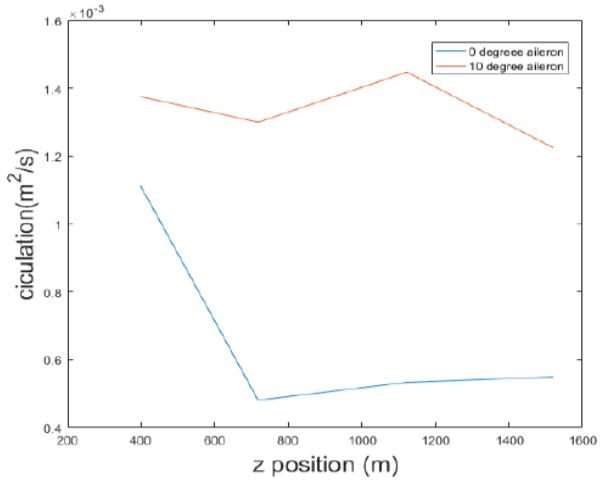

Fig 11: Circulation change along the longitudinal axis for both cases (for 0 and 10 degree aileron deflection).

5.4 The Effect of Ensemble Averaging

The concept of an ensemble average is an important one in unsteady aerodynamics. An ensemble is an imaginary collection of samples obtained from a notionally identical set of experiments, or from the same large dataset of a single experiment. Each dataset, in this case a set of 2D instantaneous velocity images projected over a certain time period, has identical fluid properties and boundary conditions, but represents the conditions over different time periods. As the flow is unsteady the details of the fluid motion will be subtly different for each sample of the ensemble. Averaging of these "ensembles" and then combining them provides an estimate of the mean of the flow property of interest, but this may dissipate important characteristics of the unsteadiness. In this case, if the spatial wander of the tip vortex or the aileron vortex is significant due to the inherent unsteadiness in the flow, the characteristics of the vortex may become dissipated over time. Whereas an instantaneous velocity field may indicate a well-defined vortex core with individual eddy features resolved in the shear layer and outer vortex, a corresponding image of the ensemble averaged flow field will present a more diffuse vortex with much of the fine detail washed out. It will, however, allow the time averaged motion of the vortex to be identified, and each image from the ensemble will be subtly different from the others, allowing some statistical information to be derived from them.

Fig. 12 provides an example of ensemble averaging of the instantaneous velocity data prior to the implementation of the three different vortex identification methods. An instantaneous image of the tip vortex core, captured with the vorticity, the Q-criterion and the Δ-criterion methods, for the case of the 10° aileron setting and the visualisation plane set at z = 398mm, is presented in Fig 12a. A corresponding set of images obtained from ensemble averaged data encompassing the first 200 time frames is then presented in Fig 12b, whilst the corresponding image for ensemble averaging of the whole 800 time frames is provided in Fig 12c.

For this particular case it is seen that the vortex core captured in the instantaneous images

using the three methods does contain some fine detail with a vortex centre where there is almost no vorticity, as expected. Ensemble averaging over the first 200 time frames results in a visible more diffuse vortex core where the fine detail is reduced and the peak values of vorticity, Q and Δ are lower than those resolved in the instantaneous image. The size and location of the tip vortex, however appears to be identical. This indicates that over the period that the ensemble average was captured there was very little movement of the tip vortex.

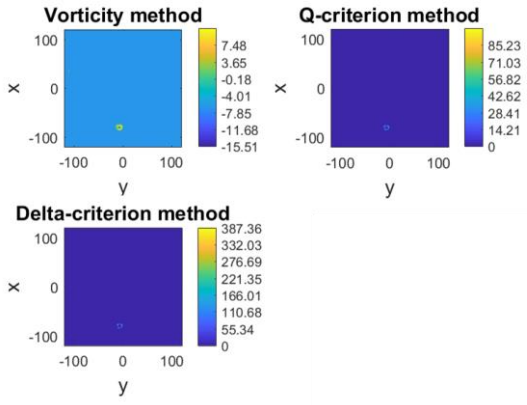

a) Instantaneous image

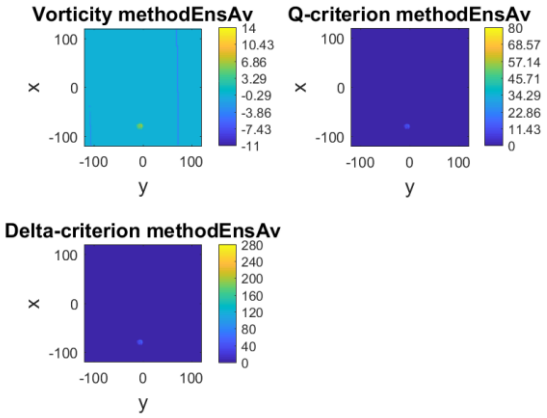

b) Ensemble average of 200 time frames

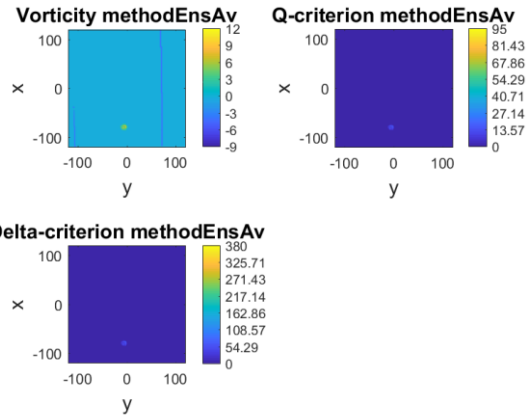

c) Ensemble average of 800 time frames

Fig 12: Vortex core capture images for the tip vortex at station z = 398mm (0.303b), aileron=10deg. U = 45m/s.

If significant motion had been present the vortex would have appeared to be much bigger in extent and much more diffuse. It is important to note that when this ensemble average image is compared with one with the same time period but later in the time history, the image appears very much the same, but with microscopic differences typical of the random nature of fluid turbulence. This is a property of ensemble averaging.

The same trends can be discerned in the images for the ensemble average over the full 800 time frames. Again the tip vortex appears in the same location with the same size, but is seen to be further diffused and with even lower peak values of vorticity, Q and Δ.

The conclusion is that for this particular vortex, at the 45m/s flow condition and at this particular *z*-location downstream of the wing tip trailing edge, there is very little discernible unsteadiness in the vortex core. At locations further downstream, however, vortex unsteadiness may well appear as the vortex ages into the far wake, and as this dataset is further analysed, the method of ensemble averaging is expected to help identify this phenomena which, together with the instantaneous data and mathematical methods such as Proper Orthogonal Decomposition (POD), will help to provide more insight into the unsteadiness of wake vortices.

6 Conclusions

The near field of the wing wake has been studied by post-processing SPIV data obtained from an experiment. The methodology of post processing the PIV data has been analysed, finding the outliners, replacing missing data and smoothing the data, vortex identification and vortex centre identification. The vorticity method is a relatively easy method to use, however a threshold value for the vortex core boundary is hard to identify. The Δ-criterion is a less strict method which will increase the size of the vortex core. The other methods show the same vortex core area. As the Q-criterion method is easy to use, this combined with the vorticity method is utilized in this paper. Note that an adjustment is required on the Q-criterion method to reveal both the strong vortices as well as weak vortices clearly at the same time. Three vortex centre identification methods were studied. The accuracy of the velocity sign method highly relies on the mesh width. If the vortex centre exactly locates on the nodes, the error will be zero. If not, the maximum error can be 0.707 times the mesh width. The Q method is a relatively new method, which has a similar algorithm as the vorticity method. However, the error of the Q method is lower than that of the vorticity method for the same case. The accuracy of the Q method and vorticity method also relies on the mesh width. The smaller the mesh width is, the higher accuracy the Q method will have. All three methods were tested to find the vortex centre. After analysing the position of the tip vortex centre, it can be found that the tip vortex moves downwards and inwards at the same time for both cases. With aileron deployed, the interaction of the aileron vortex and tip vortex makes the tip vortex tip move further outboard and upwards, closer to the wing plane. For the zero deflection aileron case the tip vortex as well as three weak vortices, which are assumed to be caused by the leading edge slat brackets exist at z = 0.198b. The size of these three weak vortices decreases rapidly downstream. At $z = 0.275b$, only one of the three weak vortices remained. At $z = 0.582b$, all the weak vortices had disappeared. During this process, the strength and size of the tip vortex decreased to a minimum at $z = 0.275b$, after which its size and strength increased. As for the deployed aileron case, the tip vortex, the aileron and the two vortices caused by the leading edge slat brackets exist at $z = 0.198b$. These two weak slat bracket vortices dissipate rapidly. The aileron vortex rotates around the tip vortex clockwise. The merging process completes before $z = 0.429b$. The size of the tip vortex does not change during this process. The maximum vortex strength appears at $z = 0.429b$, after vortex merging. Minimum circulation appears at $z = 0.275b$ for the aileron off case, which corresponds with the minimum vortex core size. The maximum circulation appears at $z = 0.429b$ for the deployed aileron case, after the merger of the tip vortex and aileron vortex.

Ensemble averaging of the instantaneous velocity fields revealed that the tip vortex in the near wake, for the 10^o deployed aileron case, was practically steady with no vortex core motion over time.

References

[1] Giuni, M. Formation and early development of wingtip vortices, University of Glasgow, PhD Thesis, 2013.

[2] Robinson, S. K., Kline, S. J. & Spalart, P. R. Statistical analysis of near-wall structures in turbulent channel flow. In Proc. Zoran P. Zaric Memorial International Seminar on Near Wall Turbulence, (ed. S. J. Kline & N.H. Afgan), pp. 218-247, Hemisphere, May 1988.

[3] Babiano, A., Basdevant, C., Legras B., and Sadourny R. Vorticity and passive-scalar dynamics in two-dimensional turbulence, *J. Fluid Mech*, 183 pp 379-397, 1987.

[4] Metcalfe, R. W., Orszag, S. A., Brachet, M. E., Menon, S. & Riley, J. J. Secondary instability of a temporally growing mixing layer. *J. Fluid Mech*, 184, 207-243, 1987.

[5] Melander, M. V., Zabusky, N. J. & McWilliams, J. C. Symmetric vortex merger in two dimensions: causes and conditions. *J. Fluid Mech*, 195, pp 303–40, 1988.

[6] Green SI, *Fluid Vortices*. Dordrecht: Kluwer, ed 1995

[7] Jeong, J. & Hussain, F. On the identification of a vortex. *J. Fluid Mech*, 285, pp 69–94, 1995.

[8] Raffel, M., Willert, C.E., Wereley, S., Kompenhans, J. Particle Image Velocimetry: A Practical Guide

[9] Moin, P., Adrian, R. J. & Kim, J. Stochastic estimation of organize structures in turbulent channel flow. In Proc. 6th Turbulent Shear Flow Symp, Toulouse, pp. 16.9.1-16.9.8, 1987.

[10] Crow, S.C. Stability theory for a pair of trailing vortices, *AIAA Journal*., 8, pp. 2172-2179, 1970.

[11] Uk.mathworks.com. 2017. Interpolate 2-D or 3-D scattered data - MATLAB griddata - MathWorks United Kingdom. Available at: https://uk.mathworks.com/help/matlab/ref/griddata.html?searchHighlight=griddata&s_tid=doc_srchtitle

[12] Garcia, D., Robust smoothing of gridded data in one and higher dimensions with missing values. *Comput. Stat. Data. Anal*. 54, 1167e1178, 2010.

[13] Garcia, D., A fast all-in-one method for automated post-processing of PIV data. *Exp. Fluids*., 2010

[14] Wang, M. An assessment of the unsteady vortex wake of the Airbus Nexus wing, Cranfield University MSc Thesis, 2017.

[15] Vaclav Kolar, Vortex identification: New requirements and limitations, *International Journal of Heat and Fluid flow* 638-652, 2007.

[16] Lamb, H., Hydrodynamics, 6th Edition, Cambridge, University Press, 1932.

[17] Holmén, V. Methods for Vortex Identification, Master's Theses in Mathematical Sciences, Lund University, 2012.

6 Contact Author Email Address

Professor of Experimental Aerodynamics, Kevin P. Garry, k.p.garry@cranfield.ac.uk.

Copyright Statement